Magnetic Resonance Force Microscopy and the spin bath : towards single-spin massive-resonator entanglement and the spoiling influence of the spin bath

Voogd, J.M. de

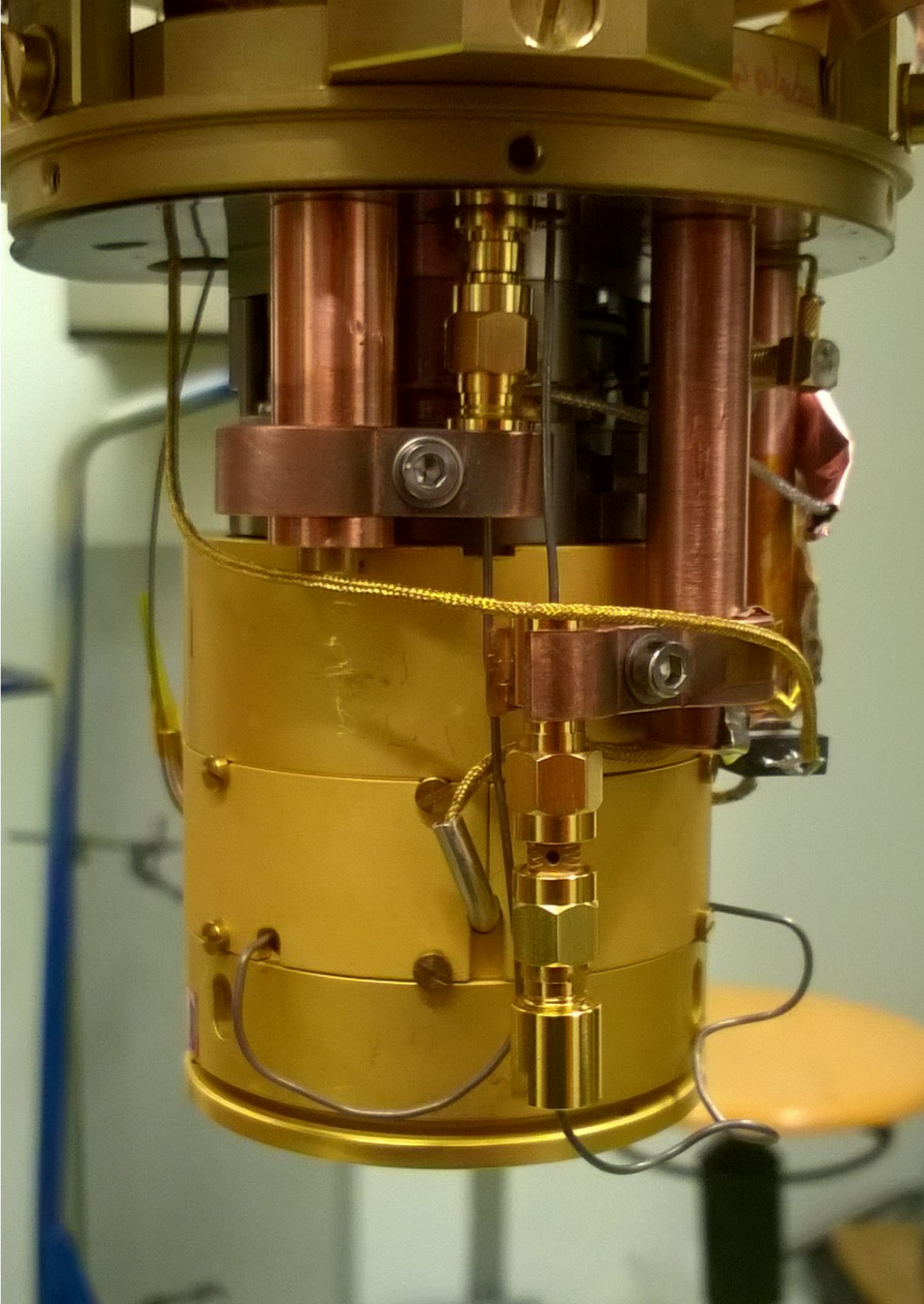

4 *MRFM on diamond*

Diamond is well known for its extreme properties. For example, it is the hardest known natural material, and at room temperature it can even have a higher thermal conductivity than that of copper. Synthetic single crystalline diamond that is grown by a Chemical Vapor Deposition (CVD) process can be extremely clean, offering < 0.05 ppb of impurity levels.[1] Most of these impurities are nitrogen atoms, sometimes accompanied by an atom vacancy (NV-center). The abundance of the impurities and the ratio of NV-centers to nitrogen impurities can be tuned by nitrogen implementation techniques and/or annealing.[2] Before applying these techniques, we expect an NV-center to nitrogen impurity ratio of 10^{-3}.[1]

[1] *The element six CVD diamond handbook*, Element Six Technologies 2015

[2] Cardellino et al. 2014

To have a coherent interaction between the MRFM-tip and an NV-center, one should have an exceptional setup that satisfies many constraints. We have combined the ideas and experiences that we collected since we started MRFM experiments in 2008 into a new setup.[3] In this chapter we describe the first experiment with this setup where we test the interaction of our cantilever's magnetic tip with the diamond sample. The experiment has two scientific goals: 1) to measure the resonance frequency shift and extra dissipation coming from the nitrogen impurities in the bulk and influence of the spins in the dirt on top of the diamond, and 2) to measure the nitrogen impurities by doing ESR using various MRFM protocols. The holy grail is to optimize the experiment in such a way that eventually a single NV-center can be

[3] See Ch. 6 for an explanation of the technical aspects.

used to create an entanglement with a mechanical resonator.[4] Here we show that the diamond provides a significant dissipation path for the mechanical resonator. In fact, we show that the dissipation cannot only be ascribed to impurities in the bulk, but also the spins on the diamond surface have a large influence - probably even larger than the bulk spins.

[4] This is the subject of Ch. 5.

THE TECHNICAL CHALLENGES faced in this experiment are numerous and a detailed explanation about our current solutions is given in Ch. 6. The experiment described in this chapter will show us the new challenges to be taken. A special feature in the design is the unmatched superconducting microwave line over the diamond that should be able to transmit ~ 10 mA currents up to a frequency of 5 GHz. The question this experiment should answer is whether the radio frequent (RF) magnetic field that is generated by these currents is strong enough to invert the targeted spins while not heating up the spin bath. Although unwanted heating seems to play a role in saturation experiments, the fields should be strong enough to do coherent spin manipulations such as adiabatic inversions, even though the bulk of our sample only has only 1 electron spin per $(24\ \text{nm})^3$. A more precise determination is left for successive experiments. In Secs. 4.1, 4.4 and 4.5 we provide analyses for the expected signals and we show that our current setup should be able to measure these. With the theoretical and experimental ingredients available, future experiments are very promising.

4.1 *Defects in diamond*

DEFECTS in diamond can be found in the lattice structure, such as vacancies, interstitial defects or dislocations, or from the abundance of impurities; i.e. atoms that are not ^{12}C. Many of the defects feature optical transitions and can therefore be studied by photoluminescence. In this chapter we are only interested in systems that interact with the mag-

netic field, regardless of their optical properties. Loubser and van Wyk[5] provided an overview of electron spin resonance (ESR) in diamond describing many defects involving nitrogen impurities. Neutral nitrogen atoms have one more electron than the carbon atoms they replace. The extra electron(s) are shared with adjacent atoms and they can form a spin system which is different from a free electron spin. However, the g-factors of the defects described in this chapter ranges only from $2.002 - 2.009$, close enough to the electron g-factor for us to assume we are dealing with simple electron spins. These spins can, however, be distorted due to the hyperfine structure which we will explore in more detail.

[5] Loubser and Wyk 1978

Given our sample,[6] and what has been reported in literature,[5,7] we can assume that the P1 and the P2 defects will have the largest contribution to the total tip-sample interaction considering their abundance and strong magnetic moment.

[6] According to the manufacturer, our sample has < 1 ppm nitrogen impurities. See next section for more information.

[7] Anderson and Payne 2006

A P1 defect consists of a single nitrogen that shares its electron with a neighboring carbon atom, featuring a simple spin-$\frac{1}{2}$ system. Due to the Jahn-Teller effect, which breaks the T_d symmetry to C_{3v}, the electron is shared predominantly with only one of the four neighboring carbon atoms. It is likely that the nitrogen is ^{14}N,[8] which has a spin-1 nucleus. The hyperfine interaction between the atom and nucleus causes a splitting of each e^--spin energy level into three levels which leads to the ESR spectrum as shown in Fig. 4.1. However, the hyperfine coupling is not purely isotropic. In our experiment we do not know the precise direction of the magnetic field at the P1 center's position, so we assume the directional dipolar coupling to be an unknown deviation from the isotropic term. This leads to a splitting of 92.2 ± 10.8 MHz. An accidental[9] neighboring ^{13}C atom with spin-$\frac{1}{2}$ can split the levels even more. The level spacing depends strongly on the precise position of ^{13}C. As the abundance of ^{13}C atoms is low, we neglect this effect for now.

[8] Natural abundance of ^{14}N is 99.64%.

[9] Natural abundance of ^{13}C is 1.1%.

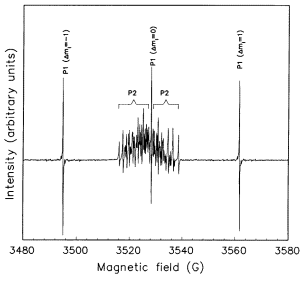

Figure 4.1: The typical 10 GHz ESR spectrum of a type Ia diamond. The P2 lines are absent in the case of Ib diamonds. *Figure reprinted from Wyk et al. 1997.*

P2 centers have a more difficult structure as the system exist of three nitrogen atoms surrounding a vacancy. Although the P2 center was one of the first to be found in EPR-experiments,[10]

[10] Smith et al. 1959

it was only after a correlation between optical N3 centers and P2 was found, that it became clear that a vacancy is part of the system.[11] The free electron is most of the time between the vacancy and the single adjacent carbon atom. This leads to a much smaller hyperfine splitting compared to the P1 center. On the other hand, the electron couples to three ^{14}N nuclei which causes a splitting of each electron spin state into 54 levels. Due to the close spacing of these levels we will treat the system as a free electron spin with a large line-broadening. Based on Fig. 4.1, we approximate the lineshape to be a Gaussian with 17 MHz standard deviation.

[11] Wyk 1982

THE RELAXATION TIMES of these P1 and P2 centers have been measured last century at various temperatures, magnetic fields, for different samples with changing spin densities, and with different techniques.[12,13] These numbers do not always coincide. Let us start by noting that at room temperature the relaxation times for P1 and P2 are approximately the same, in fact (for homogeneous fields) the T_1 and T_2 times are found to be 2 ms[12] and 3 μs[14] respectively. Moreover, the T_2 time does not seem to change much as long as the spin density is < 10 ppm, see Fig. 4.2. Similar values are measured for P1 defects in a later experiment. Takahashi *et al.*[15] did see a more or less constant T_2 time when they lowered the temperature until the thermal energy became smaller than the energy splitting. The last situation leads to much larger T_2 times; there are indications that for low enough temperatures the T_2 converges to 250 μs.[15] This effects happens upon complete polarization of the e^--spin ensemble, indicating that the limiting factor for higher temperature is the flipflop rate. On the one hand, in our experiment this rate is suppressed due to the magnetic field gradients, while on the other hand it is enhanced by the movement of the cantilever, thereby opening new ways of spin diffusion.[2] Spin diffusion, which in crystals is determined by the flipflop rate, is in MRFM effectively a form of longitudinal relaxation as the magnetization can simply diffuse out of the detection

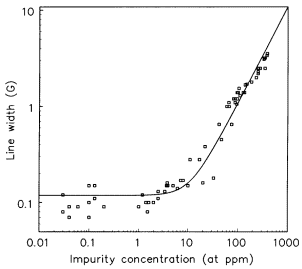

Figure 4.2: The dependence of the line width of the ESR lines of P1 centers in diamonds on the concentration of P1 and P2 paramagnetic centers. *Figure reprinted from Wyk et al. 1997.*

[12] Terblanche and Reynhardt 2000

[13] Briddon and Jones 1993

[14] Wyk et al. 1997

[15] Takahashi et al. 2008

volume. At low temperatures and homogeneous fields the T_1 time was enhanced to a value in the order of $1 - 100$ s for temperatures well below 2 K.[15] Let us take a closer look at the flipflop rate to see if the MRFM experiment changes the T_1 and T_2 significantly.

Let us assume that these flipflops are mostly between a spin and it's nearest neighbor (NN). The distance distribution to this uniform randomly distributed nearest neighbor is, for three dimensions, given by the probability density

$$\mathcal{P}\,(\text{NN at distance } r) = 4\pi\rho r^2 e^{-\frac{4}{3}\pi\rho r^3}, \tag{4.1}$$

where ρ is the spin density and r the distance between nearest neighbor spins, see also Fig. 4.3. This distribution is a measure of the distance over which the flipflops occur. A possible suppression of the flipflop rate due to magnetic field gradients[16] should be viewed in perspective of these distances.

The probability that two neighboring spins exchange magnetization is proportional to the overlapping of their lineshapes,[17,18] and is given by[19]

$$\Phi_g(\boldsymbol{r}) = \frac{\int g(\omega) g(\omega - \gamma_s \boldsymbol{r}\cdot\nabla B) d\omega}{\int g^2(\omega) \mathrm{d}\omega}, \tag{4.2}$$

where $g(\omega)$ is the normalized lineshape of the spin without taking flipflops into account. This expression is a rough estimation of the van Vleck's formula without taking into account the coupling, the relative orientation of the B-field and the temperature dependent polarization. The expression above is just enough to determine an average suppression of the flipflop rate for a given field gradient.

Comparing the typical interaction length scales, see Fig. 4.3, to our magnet with a diameter of 2.99 μm, we can assume that the spin sees a spatially *constant* magnetic field gradient G. This simplifies $\boldsymbol{r}\cdot\nabla B = r\cos(\phi)G$, where we introduced the polar angle ϕ chosen such that the poles are along the direction of the gradient. So, when $\phi = \frac{\pi}{2}$, there is no suppression ($\Phi_g = 1$) while we have an r-dependent suppression otherwise. If we take for example the lineshape of P1 centers,

[16] Namely, spins at a certain distance from each other may have a completely different Larmor frequency and therefore do not interact.

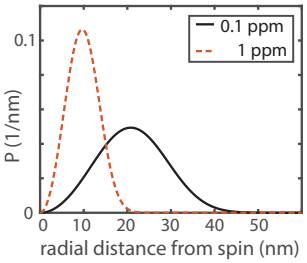

Figure 4.3: Nearest neighbor distance distribution for different spin concentrations in diamond.

[17] Abragam and Hebel 1961

[18] Vugmeister 1978

[19] Budakian et al. 2004

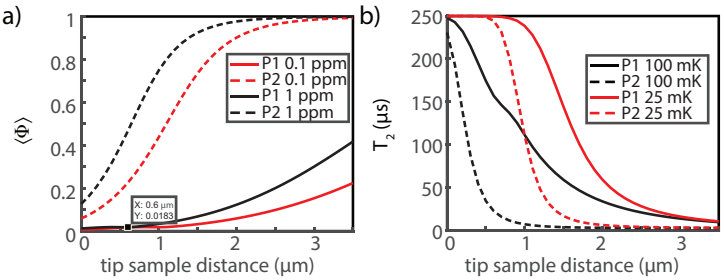

Figure 4.4: Flipflop suppression versus the distance of the spins to the magnet surface. The magnet has a radius of 1.5 μm and its magnetization is perpendicular to the displayed distance. a) Here we show the suppression factor where 0 and 1 are full and no suppression respectively. Due to the effectively broad absorption curve, P2 centers are only suppressed within a few hundred nanometer from the surface of the magnet. b) Expected T_2 time where we have taken the suppression $\langle\Phi\rangle$ for a density of 0.4 ppm spins (the same value as is measured in Sec. 4.3) for two temperatures.

see Fig. 4.5, we find a flipflop probability as shown in Fig. 4.6.

Because the flipflop rate in the homogeneous field is, under our assumptions, proportional to $\int_{\mathbb{R}^3} d^3r\, \mathcal{P}$ (NN at distance r), the average flipflop suppression per spin in the inhomogeneous field is given by

$$\langle\Phi\rangle = \frac{\int_{\mathbb{R}^3} d^3r\, \mathcal{P}\,(\text{NN at distance } r)\, \Phi_g(\boldsymbol{r})}{\int_{\mathbb{R}^3} d^3r\, \mathcal{P}\,(\text{NN at distance } r)}, \tag{4.3}$$

where $\langle\Phi\rangle = 0$ means complete suppression. We calculated this factor for spins beneath our MRFM-tip,[20] see Fig. 4.4a. The same can be done for P2 centers that we estimate to have a Gaussian lineshape with a standard deviation of about 17 MHz, see dashed lines in Fig. 4.5. Also for P2 centers below the MRFM-tip we show the average suppression in Fig. 4.4a.

[20] NdFeB magnet with a diameter of 2.99 μm and a remanence of $\mu_0 M = 1.15$ T.

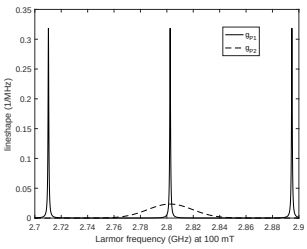

Figure 4.5: Lineshapes of P1 and P2 centers such as used in the calculations. g_{P1} is a triple Lorentzian with each FWHM $\frac{1}{3\ \mu s}$, and g_{P2} a Gaussian with a standard deviation of 17 MHz.

[21] Laraoui et al. 2012

The flipflop rate of the P1 spins in the sample is thus suppressed to less than 2% of the original flipflop rate at distances less than 1 μm below the MRFM-tip. The spin-spin relaxation time can be expressed as

$$\frac{1}{T_2} = \Gamma_{\text{flipflop}} + \Gamma_{\text{res}}, \tag{4.4}$$

where Γ_{res} is a residual relaxation rate that is expected to come from C_{13} atoms and estimated to be $\frac{1}{250\ \mu s}$.[15,21] Γ_{flipflop} is the flipflop rate which is also temperature dependent. Combining our spin suppression with the temperature dependency,[15]

we find

$$\frac{1}{T_2} = \langle \Phi \rangle \frac{A}{\left(1 + e^{\frac{\hbar \gamma_S B}{k_B T}}\right)\left(1 + e^{-\frac{\hbar \gamma_S B}{k_B T}}\right)} + \Gamma_{\text{res}}, \qquad (4.5)$$

where A is a constant of $4\left(\frac{1}{3\ \mu s} - \frac{1}{250\ \mu s}\right) \approx 1.3 \frac{1}{\mu s}$. Substituting the results of $\langle \Phi \rangle$ (Fig. 4.4a), we find the T_2 time beneath our cantilever as shown in Fig. 4.4b. Considering that our cantilever has a half period of $\frac{1}{2 \cdot 2750\ \text{Hz}} \approx 181\ \mu s$, we find that the T_2 time of the P1 spins is larger than the half cantilever period when the distance to the magnet surface is smaller than 0.4 μm when at 100 mK, and even 1.2 μm at 25 mK. This is important, because some spin manipulating pulses that we will apply[22] should coherently manipulate the electron spin for a half period.

[22] Such as OSCAR protocols, see Sec. 4.5

4.2 *Methods*

In our experiments we have used a commercially available diamond sample of $2.6 \times 2.6 \times 0.3\ \text{mm}^3$ size and < 1 ppm nitrogen and < 0.05 ppm boron concentrations.[23] One surface is polished twice to an Ra < 5 nm.[24] Cleaning the diamond subsequently in acetone, 2-propanol, fuming nitric acid and hydrofluoric acid makes sure we start the fabrication process with a clean surface and without oxides. We fabricated a Niobium Titanium Nitride (NbTiN) microwave line and a pick-up loop on top of the surface. After fabrication, the sample was exposed to atmospheric conditions for several months. Before mounting the sample it was ultrasonically cleaned in acetone, and thereafter in 2-propanol to remove organics and dust. In future experiments one might again clean the sample with hydrofluoric acid to remove possible oxygen contaminants, since oxygen compounds can contain dangling bonds and thus free electron spins, as we showed in Ch. 3.

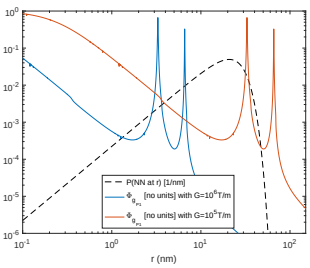

Figure 4.6: Φ_g calculated for a P1-center within a field of 100 mT and a magnetic field gradient of 1 T/μm (blue curve) and 0.1 T/μm (red curve). As a reference we plotted the average nearest neighbor distance distribution for 0.1 ppm P1 concentration.

[23] SC Plate CVD, <100>, PL *from* Element Six

[24] Second polish: scaife polishing *from* Stone Perfect

The microscope for this experiment consists of a three di-

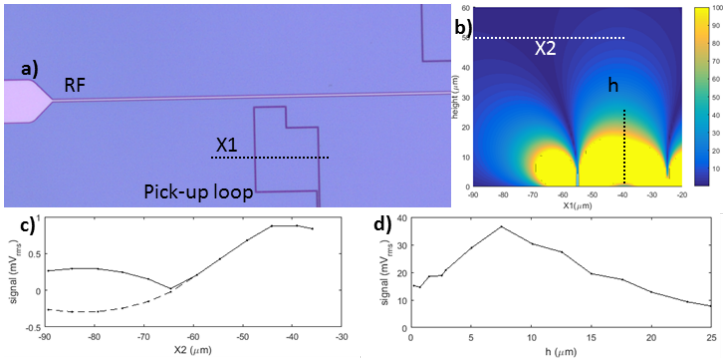

Figure 4.7: The coupling between the MRFM-tip and pick-up loop depends on the relative position. a) A microscope photo of the fabricated structures on diamond. b) Calculated signal intensity in color (arbitrary units) as function of the height between bottom MRFM-tip and sample surface, and as function of the position axis X1 as depicted in a). For visibility reasons, the signal is cutoff at 100 (yellow). c,d) The measured signal intensity as function of respectively position axis X1 and h, as denoted in b). When the cantilever passes the lines of the pick-up loop, the Lock-In measured response rotates 180°. If this phase change is taken into account one gets the dashed line in c). The zero crossing of the data taken along X2 tells the precise position of the cantilever with respect to the pick-up loop.

mensional positioning system[25] that should work down to millikelvin temperatures. The MRFM-chip, with a very soft silicon cantilever and a NdFeB magnet,[26] is mounted at the stage such that it can probe the sample. The diamond sample is glued with silver paint to a gold-plated copper sample holder. The holder is cooled via a silver strip that is thermally connected to the mixing chamber of a dilution refrigerator. A thermometer is mounted at the sample holder and a heater halfway the silver strip, such that the sample holder can be homogeneously heated to any temperature between 10 mK and 1 K.

[25] CPSHR stage *from* Janssen Precision Engineering. More info in Sec. 6.5

[26] Spring constant cantilever is $k = 48.6$ μN/m and the ball shaped magnet has a diameter of 2.99 μm, see Sec. 6.2

The movement of the MRFM-tip is detected by measuring the magnetic flux change within a pick-up loop fabricated on top of the diamond. The amount of flux change that is picked up depends strongly on the position of the tip, see Fig. 4.7. The flux is transferred to a two-stage SQUID,[27] see for more details Sec. 6.3.

[27] C6M116 *from* Magnicon

The conversion factor C from the movement of the cantilever to the SQUID output voltages can be determined in several ways.[28] We determine C by measuring the thermal noise. The surface under the curve of the thermal spectral density S_V should follow the equipartition theorem, i.e.

[28] Wijts 2013

$$\int S_V \mathrm{d}f = C^2 \int S_q(2\pi f)\mathrm{d}f = C^2 \frac{k_B T}{k}, \tag{4.6}$$

where S_q is the spectral density as defined in Ch. 1, f is the

frequency, T the temperature and k the spring constant. Of course, for this method the thermal motion of the resonator should exceed the detection noise floor. The spectral density is fitted with a Lorentzian plus an offset to account for the detection noise. The fitting parameters automatically yield the surface under the curve. Doing this at relatively high temperatures (> 100 mK) we may expect that the mode temperature is thermalized with the temperature of the environment. Once C is calculated at a certain position it may be used to check if the mode is also thermalized at temperatures below 100 mK, see Fig. 4.8.

With the conversion factor, one can calculate the detection noise floor as is done in Fig. 4.9 which shows 10 to 100 $\frac{\text{pm}}{\sqrt{\text{Hz}}}$. Surprisingly, the noise floor depends on T even at low temperatures, indicating that the detection noise is not limited by the SQUID.[29] Based on the bare SQUID characteristics one could expect a noise floor of at least an order of magnitude less.

It should be noted that for the data as shown in Figs. 4.8 and 4.9, the noise floor is suboptimal as it depends on the position of the tip, however the position of the tip was chosen based on other factors. In the future, optimizing the detection noise and the position of the cantilever could push the noisefloor (far) below 1 $\frac{\text{pm}}{\sqrt{\text{Hz}}}$.

One of the design criteria was to design the mechanical loop from the cantilever holder to the sample as stiff as possible, see also Sec. 6.5. Avoiding the mechanical resonances or moving them to (much) higher frequencies than the cantilever frequency prevents interference with the cantilever mode and thus with the force signal. Unfortunately, resonances outside the mechanical loop can also interfere as these modes accumulate to an interfering signal, such as can be seen in Fig. 4.8 as a deviation of the noise temperature from the bath temperature. The peak at 0.7 K for a tip-sample distance of 20 can be ascribed to the temperature de-

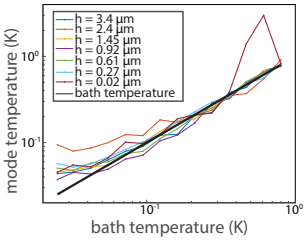

Figure 4.8: Thermalization of the cantilever to the environment versus temperatures for different heights. The data should follow the large black line in case of perfect thermalization, however, the mode temperature saturates at about 50 mK. The data is measured at different positions and is the same as used in Sec. 4.3

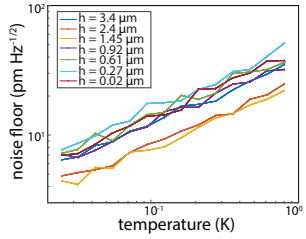

Figure 4.9: Movement detection noise floor around the cantilever's resonance frequency from the same data as Figs. 4.8 and 4.10.

[29] Due to the currents through the shunt resistors in a DC-SQUID, one can, as a rule of thumb, expect a saturation of the SQUID noise below 300 mK.

pendent frequency shift that shifts the resonator's resonance frequency over an external resonance peak. The mechanical mode can interfere via pressure waves (sound),[30] or via electromagnetic effects.[31] The disturbing signal can also come from noise sources.[32] All of these signals can increase the stored energy in the cantilever motion. If the noise source is coherent, the excess motion can be compensated using feedback schemes employing for example Kalman filters. When the noise source is not coherent (including thermal noise) one can simply feed the signal phase-rotated back into the device.[33] The maximum suppression of the motion is restricted by the detection noise floor.

In this first experiment, however, we practically shifted the resonance frequency to an area where the spectrum was clear of other resonances and where the mode temperature would follow the environment temperature well. The resonance frequency can be shifted due to the repulsion of some trapped flux inside the pick-up loop.[34]

[30] e.g. modes in mass spring systems that act as tuning forks for some frequencies

[31] e.g. resonating wirebonds attached to the sample

[32] e.g. turbo pumps(coherent) or the hammering from the pulse-tube cooler (not coherent at high frequencies)

[33] Vinante et al. 2012

[34] Unlike the repulsion due the Meissner effect of the superconducting line itself, such as Wijts 2013 calculated, we believe our superconducting lines are so small that the largest effect will be due to some trapped flux inside the loop.

4.3 *Equilibrium dynamics*

We approached the sample and measured the cantilevers response at different heights for various temperatures. With this data we can verify if the theory as described in Ch. 2 also applies to the spins in our diamond sample, just like we tested this on silicon in Ch. 3. The temperature and position-dependent shifts in resonance frequency and changes in the Q-factor can tell the densities of spins with T_1-times comparable to or larger than the resonator period.

After determining the tip-height by softly touching the sample, we started a temperature sequence at a tip-sample distance (height) of 3.4 μm. Each subsequent measurement we moved closer to the sample and also moved in lateral position until the resonator is in a clean spectral area. This was to prevent that external excitations excite the resonator. Due to the tilt of the sample, we introduced here some uncertainty in

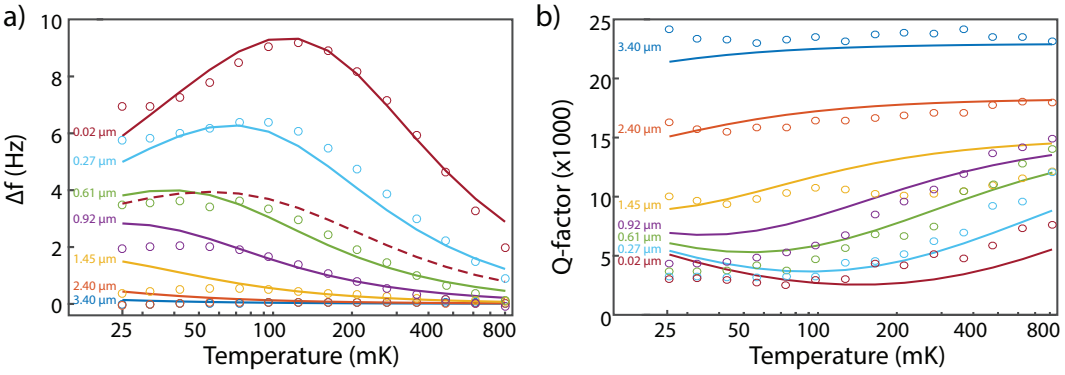

Figure 4.10: Data (circles) and theory (lines). a) Shows the shift in resonance frequency and b) how the Q-factor changes over temperature, for different heights. For the curves (solid lines) we used the 'simultaneous' values from Tab. 4.1. The dashed lines show the contribution from the bulk spins inside the diamond only.

the height. As a reference, we measured the height after the measurement series again and found a difference of 200 nm over a lateral distance of about 3 μm and used this value.[35] The results were obtained at seven heights between 3.4 μm and 20 nm, and 14 temperatures logarithmically spaced between 25 and 800 mK.

[35] The last measurements were closest to the surface, and thus for these it is most important to have a correct value. The last four measurements (0.02 – 0.92) were also laterally close to each other (within 0.4 μm distance).

For the free electron spins in the bulk of the diamond (P1 and P2 centers) we expect to have a large relaxation time $T_1 \gg \frac{1}{\omega_0}$, as explained in Sec. 4.1. Hence the theoretical function for the shifts due to the bulk spins become

$$\begin{aligned} \Delta f_{\text{bulk}} &= \frac{f_0}{2k}\,\rho\, C_{\text{bulk}}, \\ \Delta\frac{1}{Q}_{\text{bulk}} &= 0, \end{aligned}$$

$$\text{with } C_{\text{bulk}} = \frac{\mu_e^2}{k_B T}\int_{\mathcal{V}_{\text{bulk}}} \mathrm{d}^3 r \frac{\left|\boldsymbol{B}'_{||\hat{\boldsymbol{B}}_0}\right|^2}{\cosh^2\left(\frac{\mu_e B_0}{k_B T}\right)}, \tag{4.7}$$

where $f_0 \equiv \frac{\omega_0}{2\pi}$ is the resonance frequency before the shift, ρ the bulk spin density, μ_e the free electron magneton.
However, we noticed that the Q-factor decreases significantly from $> 30\,000$ at a large distance to about 2500 at 20 nm and 71 mK. The decrease is less than what was obtained on silicon in Ch. 3, but still a clear sign that spins must be present with a T_1 similar to $\frac{1}{\omega_0}$. Therefore we include a surface spin density

in our analysis. The additional shifts due to the surface spins are given by

$$\Delta f_{\text{surface}} = \frac{f_0}{2k}\,\sigma\, C_{\text{surface}} \frac{(\omega_0 T_1)^2}{1+(\omega_0 T_1)^2},$$
$$\Delta \frac{1}{Q}_{\text{surface}} = \frac{1}{k}\,\sigma\, C_{\text{surface}} \frac{\omega_0 T_1}{1+(\omega_0 T_1)^2},$$
$$\text{with } C_{\text{surface}} = \frac{\mu_e^2}{k_B T} \int_{\mathcal{V}_{\text{surface}}} \mathrm{d}^2 r \frac{\left|\boldsymbol{B}'_{||\hat{\boldsymbol{B}}_0}\right|^2}{\cosh^2\left(\frac{\mu_e B_0}{k_B T}\right)}, \quad (4.8)$$

where σ is the surface spin density.

THE FUNCTIONS Δf_{bulk} and $\Delta f_{\text{surface}}$ are not completely independent, which makes it hard to fit them simultaneously.[36] Therefore we fixed ρ,[37] and fitted σ and the T_1 of the surface spins over the temperature traces, for the each height. Next, we modified ρ until the average fitting error was minimized. The results are given in table 4.1, as well as the other system parameters. As we had to move the resonator laterally to shift the resonance frequency to cleaner spectral areas, f_0 changes per height. We calculated f_0 by extrapolating the measured frequency shift data to higher temperatures.[38]

[36] The fitting of the functions separately is a very robust procedure and largely independent of the starting point.

[37] We first fitted ρ (and the surface spins) at 20 nm height, and used this ρ as an initial value for minimizing the simultaneous fitting error over all traces.

height (μm)	ρ (ppm)	σ (spins/nm^2)	$T_{1\ \text{surface spins}}$ (ms)	f_0 (Hz)
simultaneous	0.40	0.059	0.85	—
0.02	0.4	0.058	0.99	2624
0.27	*(0.4)*	0.066	0.83	2618
0.61	*(0.4)*	0.058	0.53	2613
0.92	*(0.4)*	0.043	0.31	2606
1.5	*(0.4)*	—	—	2541
2.4	*(0.4)*	—	—	2629
3.4	*(0.4)*	—	—	2684

parameters	k (μN/m)	⊘ magnet (μm)	$\mu_0 M$ (T)	μ_s (J/T)
	48.6	2.99	1.3	$9.27{\cdot}10^{-24}$

Table 4.1: The fitting values for each trace. Note that ρ was only fitted to all traces simultaneously. For heights > 1 μm the fitting procedure did not work. Note that f_0 is separately calculated from the data.
The second table shows the known system parameters; see also Sec. 6.2.

[38] This produces the same results as when we left f_0 as a fitting parameter, however, calculating f_0 separately seems more robust.

THE FITTING did not work for heights 1.5 to 3.4 μm, presumably due to the low amount of spins,[39] making other long range effects more significant: pure diamond is insulating at any temperature which could lead to charging effects and therefore larger electrostatic interactions[40] compared to the

[39] According to our interpretation, the diamond has fewer surface spins than found on SiO, resulting in a higher Q in Fig. 4.10 than in Fig. 3.3.

[40] Kuehn et al. 2006

experiment on silicon.
Next, we choose one initial value for ρ, σ and T_1 for all data, and changed these values to minimize the squared error over all traces simultaneously. The results, as shown in Tab. 4.1, turn out to be independent of the initial values if they are chosen within an order of magnitude difference of the individual fit values. The data and the theoretical lines with the simultaneous fit values are shown in Fig. 4.10.

We have measured the equilibrium interaction from the MRFM-tip with the spins in the bulk and at the diamond surface. We have found the diamond bulk spin density to be 0.4 ppm, the surface spin density 0.06 $\frac{\text{spins}}{\text{nm}^2}$, and a T_1 time of the surface spins of a bit less than a millisecond. We can conclude that the surface spin density on diamond is much lower than on silicon, as expected.[41] Combining this with the knowledge that the sample has been exposed to air for about a year, we anticipate that by cleaning and/or passivating the surface thoroughly, the surface spin density can be reduced to non-disturbing values. What remains is the frequency shift due to the bulk spins only as shown by the dashed lines in Fig. 4.10a. The effect from the bulk spins on the Q-factor should be very small because of the very long T_1 times.

[41] Myers et al. 2014 found a surface spin density of 0.04 $\frac{\text{spins}}{\text{nm}^2}$ which is relatively close to our 0.06.

4.4 *Spin resonance I: saturation*

Saturation is a fairly simple protocol that works in MRFM for samples with spins that have a T_1 time much larger than the cantilever period.[42] Referring to Sec. 2.1, we know that when the saturation condition Eq. 2.6 does not apply for sufficiently long times, i.e. $\pi\gamma_e^2 B_1 T_1 g(\omega) \gg 1$, the spins will loose their net magnetization. Here γ_e is the gyromagnetic ratio, and B_1 is the amplitude of an oscillating magnetic field with frequency ω. If we apply this B_1-field externally, by means of the RF-wire, we can excite a specific resonance slice. The only requirement is that B_1 is strong enough and the

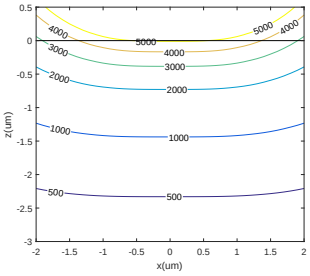

Figure 4.11: Some resonance slices indicated by their free electron spin Larmor frequency in MHz. The distance between sample (at zero height) and the surface of the tip is 0.5 µm. Here z points out of plane of the sample, and x in the direction of the magnetization.

[42] Note that for $T_1 = \mathcal{O}\left(\frac{1}{\omega_0}\right)$ we can use the equilibrium dynamics to measure T_1.

pulse long enough. The precise duration and strength, as well as the magnetic field gradient, will determine the resonance slice thickness, as explained in detail by Wagenaar.[43] For now we will assume a constant slice thickness.

[43] Wagenaar 2017

FIG. 4.11 SHOWS some of the resonance slices when the tip is positioned at a height of 0.5 µm. This is the distance at which we tried the experiment as described in this section and the next.

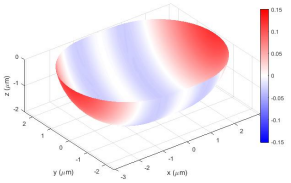

Figure 4.12: Resonance slice indicating which spins give positive or negative frequency shifts. Here, the magnetic field strength is 100 mT, the height is 0.5 µm and T_1 is taken to be infinite.

Within the resonance slice, not all spins contribute equally to the frequency shift of the cantilever; in fact, some spins produce opposite frequency shifts, see Fig. 4.12. Given an RF-frequency, a temperature, a T_1 and a T_2 time, and the other standard system parameters, we can integrate over the surface of the resonance slice to retrieve the total frequency shift per slice thickness. To get the frequency shift for P1 and P2 centers, we convolve this curve with their lineshapes. The results are shown in Fig. 4.14a.

THERE ARE TWO MAJOR PROBLEMS we encountered when we tried to apply this protocol. The first is the signal strength; due to the low density of spins the signal is just below the fluctuations in the measured frequency of the force sensor which are higher than we wanted due to the excess SQUID noise, see Sec. 4.2. This is something that could be solved for a future experiment. Further, we noticed that the RF-source produces large RF-leakage, such that it can still heat up the spin bath.[44] Finally, applying RF-pulses with frequencies higher than 5 GHz can give comparable frequency shifts as RF-frequencies at for example 4 GHz, which does not agree with Fig. 4.14a. This could be the result of other spin-like level systems at the surface of the diamond that respond to higher frequencies, but it could also be a simpler reason: the direct heating of RF-current or field. We have found that the dissipated power of a pulse in the sample is 0.9 µW/mA, see Fig. 4.13. Although the sample's temperature is kept within a few mK from the setpoint value, the question is if the pulse

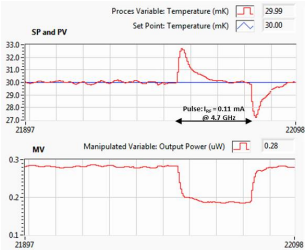

Figure 4.13: Screenshot of experiment to test pulse power. The sample holder is kept at constant temperature (PV) by a PID controller when we apply an RF-pulse. The difference between the heater power (MV) before and during the pulse should be the power the pulse induces.

[44] The source produces about −40 dB leakage, so when the amplitude before the output is set to 10 dBm, but the modulation such that no power should come out, the output still transmits −30 dBm.

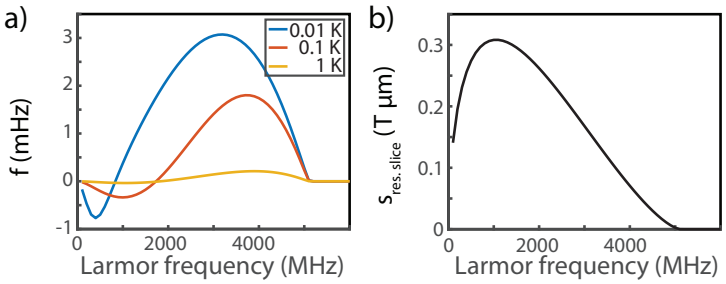

Figure 4.14: Calculated signals for magnetic resonance protocols for a MRFM-tip at a height of 500 nm above our diamond sample. a) Shows the frequency shift per resonance slice of 10 nm thickness after applying a saturation pulse (making the spin-temperature infinite locally). The results are shown for a free electron spin; in this graph the results for P1 or P2 deviate less than 1% from the free electron spin. b) The signals obtained with the protocols as described in Sec. 4.5 are proportional to $\left|\boldsymbol{B}'_{\|\hat{\boldsymbol{B}}_0}\right|$ integrated over a resonance slice surface. Here we show the value of this integral for different resonance slices.

doesn't also drive the local spin temperature outside the resonance slice much higher.

4.5 *Spin resonance II: spin coherence*

In this section we describe two measurements which directly measure the force from the spins on the cantilever. The two methods in this section are distinguished by the way the spin manipulates the cantilever; the first measures the extra induced movement when the resonator is only thermally excited, while the second measures a frequency shift when it is driven in a Phase-Locked Loop (PLL).

The spin-manipulating protocols for both measurements are based on the principle of adiabatic spin inversion,[45] which is necessary due to the inhomogeneous B_1-field. Unlike partial-Rabi-cycle sequences,[46] an Adiabatic Rapid Passage (ARP) flips the spin, independent of the precise B_1-field strength as long as it satisfies the following conditions:

$$\frac{1}{T_2} \ll \frac{\mathrm{d}}{\mathrm{d}t} \tanh\left(\frac{B_1(t)}{B_0(t) - \frac{\omega_{RF}(t)}{\gamma_e}}\right) \ll \gamma_e B_1, \qquad (4.9)$$

i.e. a pulse must be designed such that it sweeps through the resonant condition at a rate faster than the T_2 dephasing rate, but slower than the Rabi frequency that is set by the amplitude of the pulse.

For the first measurement (the force measurement) we use

[45] Slichter 1990

[46] Such as combinations of $\pi/2$ and π-pulses that are used to measure spin echoes.

ARP in which both the amplitude B_1 and the frequency ω_{RF} of the B_1-field are changed. For the second measurement, which we will call the frequency shift measurement, we use OScillating Cantilever-driven Adiabatic Reversals (OSCAR) where ω_{RF} is kept constant while the motion of the magnetic tip causes the spins to be swept through resonance.[47]

[47] Stipe et al. 2001b

For the force measurement, the cantilever is only very sensitive to the Fourier components of the spin force around the cantilever's resonance frequency. More precisely, given the MRFM tip's susceptibility χ, the measured voltage is

$$V_{\text{signal}}(\omega) \propto \tilde{q}(\omega) = \chi(\omega)\tilde{F}(\omega), \tag{4.10}$$

where $\tilde{F}$ is the Fourier transform of

$$F(t) = \langle \boldsymbol{\mu} \rangle_{ARP} \cdot \boldsymbol{B}' \text{sgn}(\cos(\omega_S t)), \tag{4.11}$$

$$\approx \frac{\pi}{4} \mu_{ARP} \left| \boldsymbol{B}'_{\| \hat{\boldsymbol{B}}_0} \right| \cos(\omega_S t). \tag{4.12}$$

Here μ_{ARP} is the net magnetization and ω_S the frequency of the spin rotating 360°. As a spin will flip 180° during a single ARP, two pulses are needed to return the longitudinal magnetization to equilibrium position.[48] In the last step we have taken the Fourier components around ω_0, which is valid when we choose $\omega_S \sim \omega_0$. For the total signal we integrate over the resonance slice and find[49]

$$q(t) = \int_{\mathcal{V}_{res.slice}} \rho \, \mu_{ARP} \left| \boldsymbol{B}'_{\| \hat{\boldsymbol{B}}_0} \right| d\mathcal{V} \quad \times$$
$$\frac{1}{k} \left(2 \frac{\omega_0 - \omega_S}{\omega_0} \cos(\omega_S t) + Q \sin(\omega_S t) \right), \tag{4.13}$$

where ρ is the bulk spin density. Thus when we choose the pulse sequence such that the spin force follows a reference sinusoid with $\omega_S = \omega_0$, then all spin signal will be in the quadrature component (Y) of the measurement signal, while the in-phase component (X) only contains thermal motion. Before the sequence, the X and Y components contain on average the same amount of thermal energy (i.e. $\langle Y^2 \rangle = \langle X^2 \rangle$).[50] Therefore, during the pulse sequence, the pure spin signal is $\sqrt{\langle Y^2 \rangle - \langle X^2 \rangle}$.

[48] Thus the pulse frequency is not equal to ω_0 (but $2\omega_0$) and therefore there should be little crosstalk between RF-pulse and cantilever.

[49] Similar to the derivation of Eqs. 1.5-1.6. See also Peddibhotla 2013

[50] Here energy means signal squared.

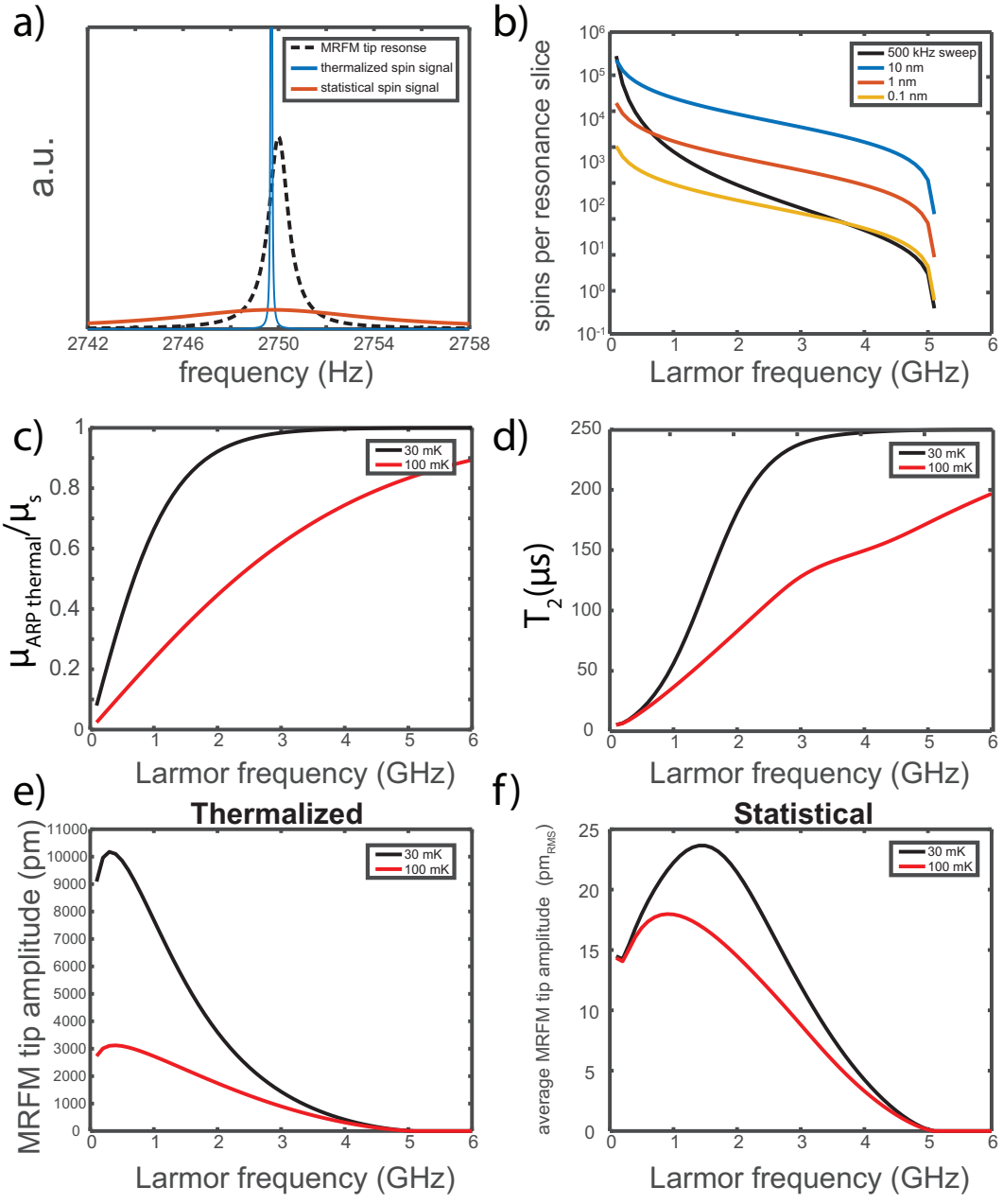

Figure 4.15: Theoretical expectations of the ARP experiment outcome. a) Spectral densities of the signals of thermally and statistically polarized spins compared to the linear response of the MRFM-tip. ω_S is set to 2749.9 while ω_0 is 2750. b) Number of spins in a resonance slice of fixed thickness, and a resonance slice where the width is determined by the frequency sweep range of the ARP pulse (500 kHz FWHM in the first ARP experiments). c) Net magnetization of thermalized spins as function of the resonance slice's Larmor frequency. d) Estimated T_2 time which is calculated as described in Sec. 4.1. e) The expected MRFM amplitude if the spin inversion autocorrelation time is longer than the duration of a single experiment e.g. the thermally polarized regime. f) Expected RMS averaged amplitude of the MRFM tip if the magnetization is statistically determined.

The advantage of measuring the energy X^2 and Y^2 rather than X and Y is that the sign of initial magnetization does not matter. Therefore, this method still works if the initial magnetization is not determined by thermalization but by statistical polarization. This statistical magnetization can be the dominant term for the net magnetization in small ensembles at temperatures $k_B T > \mu_s B_0$.[51] So, although we will try to stay in the thermalized regime, statistical polarization might help us out if the spin temperature becomes too high.

[51] Mamin et al. 2003

So far, we assumed that both conditions of Eq. 4.9 are satisfied. In our experiment, however, we use ARP pulses of length $\sim \frac{1}{2f_0} \approx 180$ μs. Comparing this with the T_2 values in Fig. 4.4b, we notice that our ARP protocol with pulses this long, and at 100 mK, should only work within about 0.5 μm distance from the tip. More precisely, for spins at resonance, the net magnetization after an ARP pulse is $|\mu_{after}| = |\mu_{before} e^{-\frac{K}{T_2}}|$,[52] where K is a pulse shape dependent parameter and proportional to the single pulse duration.[53] The success rate, or fidelity, of one spin inversion is thus $e^{-\frac{K}{T_2}}$. However, we apply a series of these inversion pulses. A typical sequence length is $\frac{Q}{f_0} \approx 1$ s. Longer sequences would not be beneficial as the resonator cannot collect more spin signal due to the cantilever's relaxation time (and because of reasons explained below). On the other hand, shorter sequences do not use the full capacity of the resonator.[54] In our case, this means we have to apply a series of about 6000 spin inversion pulses. To ensure that a significant amount of net magnetization will create a spin signal during the pulse sequence, a single spin inversion fidelity should be about 0.9999. This means that to measure the pure spin signal curve of Fig. 4.14b, the pulse dependent parameter K must be smaller than $10^{-4} T_2$ for all spins in the resonance slices that we want to measure.

[52] Norris et al. 1991

[53] Hajduk et al. 1993

[54] Another way to see this is that for series shorter than $\frac{Q}{f_0}$ the spectral leakage of the spin signal is wider than the resonator's resonance peak, so the spin signal is not optimally transduced.

During our first ARP experiments,[55] it is not likely that we satisfied this condition. In fact, based on similar pulse shapes[53] we estimate K to be as large as 30 μs, while 250 μs $> T_2 >$ 3 μs as explained in Sec. 4.1. This means that soon after the

[55] Upon finishing this thesis consecutive experiments are performed that might have better conditions.

pulse sequence is started, the average thermal net magnetization is reduced to insignificant values. However, statistical polarization helps us out as the average magnetization amplitude[56] due to statistical polarization would be about $\mu_{ARP} \propto \sqrt{N}\mu_s$, where N is the number of spins inside the resonance slice. The slice thickness can be set by the frequency sweep range of the pulse with a lower limit set by the resonator's RMS displacement. In our case this limit is on the order of 0.1 nm due to thermal excitations, but can increase during the pulse due to the force of the spins driving the resonator. See Fig. 4.15b for a comparison of the number of spins per resonance slice when the thickness is fixed or set by a frequency sweep of 500 kHz.

[56] With average magnetization amplitude we mean the root mean squared (RMS) magnetization. We naturally measure the RMS magnetization if we take the mean of the measured X^2 and Y^2 signal (and take the square root afterwards).

When spin inversions are imperfect, not only does the amplitude of the spin signal change, also the force becomes distributed over a frequency range due to the limited autocorrelation time. As the fidelity of a single spin inversion is e^{-K/T_2} and the spin is flipped with frequency $2\frac{\omega_S}{2\pi}$, the net magnetization averages out as $\langle \mu_{ARP}(0)\ \mu_{ARP}(t)\rangle \propto e^{-t/\tau}$ with $\tau \equiv \frac{\pi T_2}{\omega_S K}$ the autocorrelation time, and where we assumed $T_1 \gg \tau$. The autocorrelation time tells us that the spin signal has a frequency width of $1/\tau$ and also that if it is larger than the ARP sequence duration, we are in the thermal magnetization regime. While if τ is much smaller than the sequence duration, we are in the statistical polarization regime.

Next, we calculate the autocorrelation of the single-spin force of Eq. 4.12 by substituting the average autocorrelation of a single spin into μ_{ARP} that we have found to be $\mu_s^2 e^{-t/\tau}$ for $t > 0$. We can use the Wiener-Khinchin theorem to find the force power spectral density (averaged for a single spin) to be

$$S_F(\omega) = \left(\frac{\pi}{4}\mu_s \left|\boldsymbol{B}'_{\|\hat{\boldsymbol{B}}_0}\right|\right)^2 \tau \frac{1 + i\omega\tau}{1 + (\omega_S\tau)^2 - (\omega\tau)^2 + 2i\omega\tau} \tag{4.14}$$

$$\approx 0.4\ \tau \left(\mu_s \left|\boldsymbol{B}'_{\|\hat{\boldsymbol{B}}_0}\right|\right)^2 \qquad \text{for } \omega \approx \omega_S. \tag{4.15}$$

We only need the value of the force around the resonance peak of the transducer (the MRFM-tip). The force signal is

spectrally widespread compared to the MRFM-tip if $\tau \ll \frac{Q}{\omega_S}$ and therefore can be approximated linearly, see Fig. 4.15a. The approximation is valid up to a factor of $\sqrt{2}$ depending on the precise value of τ, which should be accurate enough for our heuristic approach.

The derivation of the power spectrum of the MRFM-tip movement is similar to Eqs. 1.7-1.11, and leads to

$$S_q(\omega) \approx 1.4 \, \frac{T_2}{K} \, \frac{Q}{k^2} \int_{\mathcal{V}_{res.slice}} \rho \left(\mu_s \left| \boldsymbol{B}'_{\|\hat{\boldsymbol{B}}_0} \right| \right)^2 d\mathcal{V} \quad \times \\ \frac{\frac{\omega_0}{2\pi Q}}{(\omega_0 - \omega)^2 + \left(\frac{\omega_0}{2Q} \right)^2}. \tag{4.16}$$

Note that in contrast to Eq. 1.11 the phase is still well defined $\phi(\omega) = \text{atan2}\left(\frac{-\omega_0 \omega_S}{Q}, \omega_0^2 - \omega_S^2 \right)$ with respect to the phase of the spin force. For the total spin signal of the resonance slice we have to integrate over the power spectrum. The last line of Eq. 4.16 integrates to unity, leaving us with the first line only.

To conclude the differences between the statistical and thermally polarized experiments, we find that the regime is determined by the autocorrelation time of the net magnetization $\tau = \frac{\pi T_2}{\omega_S K}$ during the ARP experiment. If τ is longer than the ARP experiment duration, which wisely would be chosen of the order $\frac{Q}{\omega_0}$, then we are in the thermally polarized regime and Eq. 4.13 applies. Then the signal is proportional to the number of spins N in the resonance slice (Fig. 4.15b), to the gradient of B_0 in the direction of the movement of the resonator (Fig. 4.14b), and to the thermal polarization (Fig. 4.15c), which ultimately leads to Fig. 4.15e. The statistical regime applies when $\tau \ll \frac{Q}{\omega_0}$ and Eq. 4.16 applies. The final signal, the square root of the power spectrum of Eq. 4.16 integrated over frequency, is proportional to $\sqrt{N}$ (square root of Fig. 4.15b), the RMS of gradient of B_0 in the direction of the movement of the resonator, and the square root of the T_2 time (square root of Fig. 4.15d) which leads to Fig. 4.15f.

Our first ARP experiments were carried out at a height of 500 nm and a distance of 27 μm from the RF-wire. We

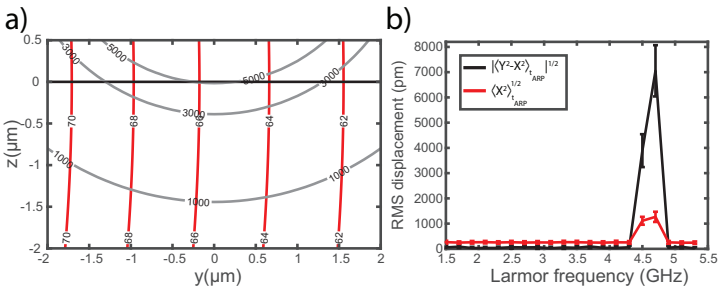

Figure 4.16: The first ARP experiments. a) The equipotential lines of constant B_1-field in kHz (red) and, as reference, some resonance slices with constant Larmor frequency in MHz (gray). b) The measured spin-force signal in black, and the average in-phase signal in red. If the ARP experiment was done in the thermal regime, red is the thermal motion$/\sqrt{2}$ plus the spectral leakage due to the finite pulse sequence duration.

applied ARP pulses of 0.63 mA through the RF-wire creating $\gamma_e B_1 \approx 66$ kHz at the position of the resonance slices, see Fig 4.16d. This B_1 is high enough to satisfy the last condition of Eq. 4.9 for all resonance slices.

For most Larmor frequencies we find that $\langle Y^2 \rangle = \langle X^2 \rangle$; except for two data points: 4.5 and 4.7 GHz have a significant signal inside the quadrature part. Reasons for these two points to appear could be: that we are suddenly in the thermal regime due to the higher field and field gradient (rather wishful thinking), that the spins from the surface add to the spin signal (not likely due to small T_2 of surface spins), resonances in the RF-wire (the peak is too broad for a single resonance in a superconducting circuit), heating of the system (not clear why only at this frequency), or that the RF leaks into the SQUID device and creates nonlinearities. Recent experiments that are outside the scope of this thesis tend to support the last hypothesis. The other data points (black points in Fig. 4.16b) are too far below the thermal signal (red signal) to show any significant spin signal.

As this analysis was only performed after the experiment, a closer determination of the spin signal with ARP is left for consecutive experiments. The RF-current lines can handle several mA, providing enough freedom to shorten the ARP pulses[57] and reveal more of the theoretical curve of Fig. 4.15e or f. Also phase measurements can be optimized by doing the quadrature measurements faster than τ and using the MRFM-tip's frequency-phase relation to suppress the influence of the thermal motion.

[57] This can be used to optimize the ARP pulse shape and thereby lower the parameter K by one or two orders of magnitude.

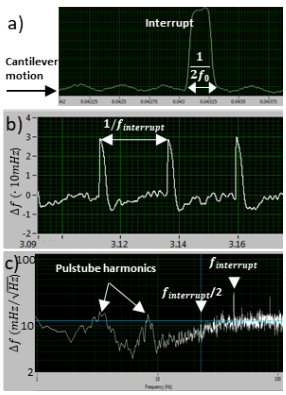

Figure 4.17: Screenshot of live data capturing during iOSCAR protocol. a) SQUID signal in time-domain, showing the cantilever movement. b) PLL frequency tracking in time domain. The sudden interrupt of the RF-signal messes up the PLL for a short while. c) PLL frequency in frequency domain. The spin signal is in the small peak at $f_{\text{interrupt}}/2$.

During the OSCAR protocol the cantilever is driven with several nanometers amplitude to use the gradient of the magnet to invert the spin each time the magnet 'passes by', causing the spin to lock, or antilock to the cantilever motion.[58] Turning the RF off for half a period should switch the locked spins to antilock and vice versa, and thereby the resonance frequency changes as there is usually an imbalance between the amount of locked vs antilocked spins. Doing this regularly and measuring the periodic change of the resonance frequency is called iOSCAR.[59] The RF can also be pulsed (piOSCAR)[60] to narrow the resonance slice, which in a follow-up experiment might also be done in view of the short T_2 time. Let us for now stick with iOSCAR. The frequency shift due to a single spin is given by[58]

$$\delta f \approx \frac{2f_0}{\pi k A} \mu_{eq} \left| \boldsymbol{B}'_{\parallel \hat{\boldsymbol{B}}_0} \right|, \tag{4.17}$$

where A is the resonator's amplitude. Of course, this δf has to be integrated over all the spins inside the resonance slice. When the interrupting frequency is $f_{\text{interrupt}}$, the magnetization changes with $f_{\text{interrupt}}/2$, and the amplitude of the frequency shift at $f_{\text{interrupt}}/2$ gives δf, see Fig. 4.17. Theoretically, this δf should follow the curve as given in Fig. 4.14b. However, for now the data as retrieved in Fig. 4.17, was too noisy to be useful. It is likely that one has to go to very short[61] piOSCAR pulses, to invert the spins within T_2.

[58] Lee et al. 2012

[59] Rugar et al. 2004

[60] Cardellino et al. 2014

[61] With respect to the cantilever period.

4.6 Conclusions and outlook

Compared to preceding experiments,[62,63] we have made notable progress in sending large RF-currents, fast temperature monitoring and controlling, and we solved the problem of very large frequency shifts.[64] However, the MRFM-experiment on diamond has also shown several points that need to be fixed or optimized such as the SQUID excess noise, RF-leakage that heats up the spin bath, and the vibrations and resonances that drive the resonator. The first two can be easily solved, but the latter needs a much better

[62] Vinante et al. 2011a

[63] Usenko et al. 2011

[64] Wijts 2013

vibration isolation, and probably a new MRFM-design.[65]

[65] More on this in Sec. 6.5

The experiment so far has been successful in obtaining spin density information of the bulk *and* the surface spins on diamond. Furthermore, we have calculated the influence from the limited T_2 relaxation time in ARP experiments. We suggest that for future experiments pulse shapes are used that ensure that the spin inversions take place with much higher fidelity.

To conclude the analysis of our resonance experiments we might say that an important factor is the quality of the spin lock which determines the bandwidth over which the spin signal is spread out. The quality of the spin lock is to a large degree determined by the duration of a single spin inversion which determines the K parameter. The duration is limited by the strength of the B_1 field. Furthermore the quality of the spin lock can be deteriorated by possible disturbances of spins in the vicinity. In the single spin experiment of Rugar et al. 2004 an excellent spin lock of longer than 1 second was achieved with a B_1 field of 0.3 mT. In their sample of quartz, the spins were generated by gamma ray irradiation with an estimated spin density of $10^{13} - 10^{14}$ cm^{-3}, or an average spin-spin distance of around 300 nm. This is significantly farther apart than the 20 nm separating the nitrogen spins in our diamond.

In the experiment of Cardellino et al. 2014 the spins implanted as a wire in diamond were studied. At 6 ppm or 10^{18} cm^{-3} (rather than our 0.4 ppm) these spins were significantly closer to each other ($5 - 10$ nm) than in our experiment, however, in the iOSCAR protocol used, they could lock the spins to the cantilever motions for more than 20 ms, even though the flip-flop time was 0.2 ms.

In our experiment we are able to generate B1 fields larger than 0.1 mT at 1 micron distance from our superconducting RF wire. We believe that we can generate spin locks for at least 20 ms. This would mean the spin signal will be spread out over a bandwidth of well below 50 Hz and therefore a single spin could become detectable in a single shot experiment.